

## Enlarging the *d*-spacing of graphite and polarizing its surface charge for driving lithium ions fast†

Cite this: *J. Mater. Chem. A*, 2014, 2, 7600

Tae-Hee Kim,<sup>a</sup> Eun Kyung Jeon,<sup>a</sup> Younghoon Ko,<sup>a</sup> Bo Yun Jang,<sup>b</sup> Byeong-Su Kim<sup>\*a</sup> and Hyun-Kon Song<sup>\*a</sup>

Lithium ion transport was accelerated within graphite by controlling its *d*-spacing as well as its functional groups. By oxidizing bare graphite under a mild condition, expanded graphites (EG\* where \* = functional groups) were obtained with increasing *d*-spacing from 0.3359 nm to 0.3395 nm as well as with functional groups formed on the plane or at the edges of graphites. The subsequent thermal reduction of EG\* led to an insignificant change of *d*-spacing (0.3390 nm), simultaneously eliminating a portion of the functional groups (EG). The enlargement of *d*-spacing reduced kinetic hindrance of lithium ion movement within the expanded graphites (EG\* and EG) by reserving more space for the ionic transport route. In addition, the activation energy of lithium ion intercalation in EG\* was reduced by surface charge polarization of graphites induced by hydrogen bonds between oxygen atoms of carbonates in electrolytes and hydrogen atoms of surface functional groups of the expanded graphites, even if the degree of graphitization decreased. Re-graphitization induced by the subsequent thermal reduction increased delithiation capacities ( $Q_{\text{dLi}}$ ) of EG as an anode for lithium ion batteries especially at high currents:  $Q_{\text{dLi}}$  at 50 C = 243 mA h g<sup>-1</sup> for EG versus 66 mA h g<sup>-1</sup> for bare graphite.

Received 23rd December 2013  
Accepted 8th March 2014

DOI: 10.1039/c3ta15360f

www.rsc.org/MaterialsA

### Introduction

Graphites have been dominantly used as an anode of lithium ion batteries (LIBs) due to their reversible structural change during lithiation and delithiation and low cost despite their relatively low capacity (theoretically, 372 mA h g<sup>-1</sup>).<sup>1</sup> As LIB technologies develop, their application areas have been gradually extended from small mobile devices to large energy storage devices.<sup>2</sup> Therefore, not only higher energy densities but also higher power densities are required. Though alloying-based or conversion-reaction-based compounds deliver higher capacities at slow charge or discharge rates than those of the intercalation-based graphites, they are significantly inferior to graphites in terms of kinetics.<sup>3,4</sup>

To increase the kinetics of lithiation/delithiation of graphites for guaranteeing high power densities, several approaches have been suggested. Park *et al.* controlled the peripheral *d*-spacing of graphite ( $d_o$ ) by edge-selective functionalization, resulting in 190 mA h g<sup>-1</sup> at 50 C.<sup>5</sup> Tossici *et al.* prepared KC<sub>8</sub>-derived graphite of a larger interlayer distance (0.341 nm) due to potassium trespassing, which improved kinetics of the subsequent lithium intercalation.<sup>6</sup>

Graphite oxides and their derivatives such as graphene oxides, reduced graphene oxides and graphene sheets were used as anodes of LIBs.<sup>7–11</sup> However, the enhancement of their capacities at low rates was focused. Also, the lithiation mechanism of the derivatives is not based on intercalation processes, which is electrochemically well-defined.<sup>9,10</sup> Enlarging the *d*-spacing into 0.6 to 0.7 nm by severe oxidation of graphites<sup>12</sup> does not result directly in kinetic improvement because the oxidation of graphites vastly decreases the electrical conductivity from 2500 S m<sup>-1</sup> for graphites to 0.021 S m<sup>-1</sup> for graphite oxides.<sup>13</sup> That is to say, electron conduction decreases significantly even if ionic movement is enhanced through the widened ionic pathways. Not the lithium ion diffusion process but the electron conduction step determines the overall rates of intercalation.

In this work, we oxidized graphites in a mild (not severe) way to guarantee (1) expanding the *d*-spacing into the inter-graphitic distance at which the  $\pi$ - $\pi$  stacking force is maintained and (2) keeping the electrical conductivity at a level of conductor without severe formation of defects to break the resonance structure of sp<sup>2</sup> hybrid configuration of graphitic planes. The resultant expanded graphites (EG\*) and their thermally annealed version (EG) were characterized and compared with bare graphites by X-ray diffraction (XRD), X-ray photoelectron spectroscopy (XPS) and Raman spectroscopy. The delithiation kinetics of EG\* and EG were proved to be superior to bare graphites under galvanostatic stimulation conditions. Differential capacity analysis and *in situ* electrochemical impedance

<sup>a</sup>School of Energy and Chemical Engineering, UNIST, Ulsan 689-798, Korea. E-mail: philiphobi@hotmail.com

<sup>b</sup>Korea Institute of Energy Research (KIER), Daejeon 305-343, South Korea

† Electronic supplementary information (ESI) available. See DOI: 10.1039/c3ta15360f

spectroscopy (EIS) revealed why the expanded graphites are excellent at high C-rates.

## Experimental

### Mild oxidation of graphite to EG\* and subsequent thermal reduction of EG\* to EG

EG\* (\* = functional groups) as an expanded and functionalized graphite was prepared from natural graphite powder (Aldrich) by the modified Hummers method.<sup>14</sup> Graphite powder (1 g), potassium persulfate ( $K_2S_2O_8$ ; 0.5 g) and phosphorus pentoxide ( $P_2O_5$ ; 0.5 g) were mixed in sulfuric acid ( $H_2SO_4$ ; 5 ml) with stirring until the reactants were dissolved. The mixture was kept in an oil bath at 80 °C for 4.5 hours. After that, the mixture was diluted with DI water and stirred for about 5 min. Solid contents obtained after filtering and washing the mixture were transferred to a drying dish and left at room temperature overnight. Potassium permanganate ( $KMnO_4$ ; 0.5 g) was slowly added as an oxidizing agent to  $H_2SO_4$  (26 ml) containing the pretreated graphite in an ice bath. It should be noted that the amount of  $KMnO_4$  used in this work is one-sixth of the amount used for synthesizing graphene oxide.<sup>14</sup> The mixture was reacted at 35 °C for 2 hours. After deionized water (46 ml) and 30% hydrogen peroxide ( $H_2O_2$ ; 2.5 ml) were added, the resultant mixture was allowed to settle and the clear supernatant was decanted. 10% aqueous solution of HCl was added into the remaining mixture with stirring and then the mixture was filtered. The resulting solid was dried in air. The dried solid was added to deionized water. Solid contents were purified from the suspension through centrifugal dialysis. The collected precipitate was dried at 60 °C in oven. The resultant expanded graphite oxide (EG\*) powder was thermally reduced in a furnace at 150 °C under an argon atmosphere. The ramping rate was fixed at 5 °C  $min^{-1}$ . EG\* was re-graphitized to EG with fewer functional groups (indicated by \* in EG\*).

### Characterization

Cold field emission scanning electron microscopy (FE-SEM; Hitachi, S-4800) was used to observe the morphology changes of natural graphite after mild oxidation and heat treatment. The crystallographic structures were studied using a high power X-ray diffractometer (XRD) and a Cu K $\alpha$  source (Rigaku, D/MAZX 2500V/PC). Functional groups of graphites were analysed by XPS (Thermo Fisher, K-alpha) and micro-Raman spectroscopy (WITec, alpha 300R). Carbon and oxygen contents were measured by elemental analysis based on the combustion method (LECO Co., TrueSpec Micro CHNS).

To characterize the electrochemical properties, CR2032 coin cells were assembled in an Ar-filled glove-box (less than 0.4 ppm of  $H_2O$  and 0.1 ppm of  $O_2$ ). A mixture composed of active material (80 wt%), poly(vinylidene fluoride) (PVDF) (10 wt%) as a binder and Super P (10 wt%) as a conducting agent were cast on Cu foil by using a doctor blade and then dried in a vacuum oven at 120 °C for 2 h. Lithium metal foil was used as a counter electrode while 1 M  $LiPF_6$  dissolved in ethylene carbonate (EC)-diethyl carbonate (DEC) (1/1, vol%) was used as an electrolyte.

Electrochemical performances were tested using a galvanostatic battery test system (WonA Tech) from 0.01 V to 1.5 V at different current rates (C-rates). Electrochemical impedance spectroscopy (EIS) was performed *in situ* during galvanostatic delithiation processes by synchronizing an applied current with sinusoidal current signals using a 300  $\mu A$  sinus amplitude in the frequency range from 50 kHz to 10 Hz. The impedance data were recorded every 10 min during delithiation at 0.1 C.

## Results and discussion

Morphological changes at a sub-micrometer dimensional level were observed upon the mild oxidation and the subsequent thermal reduction (Fig. 1). The bare graphite formed closely packed secondary particles of graphitic sheets with >15  $\mu m$  size. The secondary particles consisted of flake-like primary particles. After the mild oxidation, however, the graphitic flakes were partly exfoliated in EG\*. There were no significant differences observed after the subsequent thermal reduction from EG\* to EG.

The degree of expansion between graphitic sheets was evaluated by XRD (Fig. 2). A main peak of bare graphite detected at 26.5° along the (002) plane was very sharp, indicating that the graphite had a large domain size of crystallites with regular distance between graphitic sheets. After the mild oxidation (EG\*), the (002) peak was shifted to the lower angle and broadened. Functional groups (discussed below with Fig. 3) generated by the oxidizing agent at the edges or on the planes of graphites extend the distance between graphitic sheets

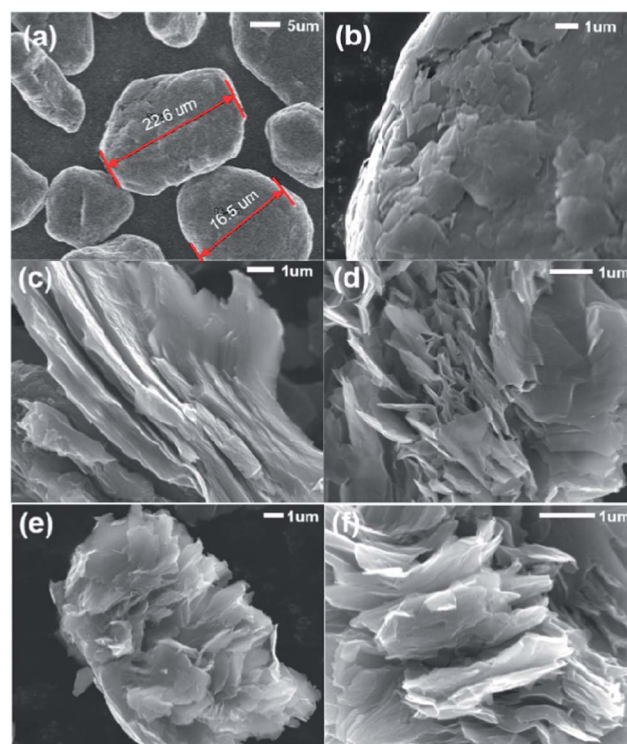


Fig. 1 Morphological characterization. SEM images of bare graphites (a and b), EG\* (c and d) and EG (e and f).

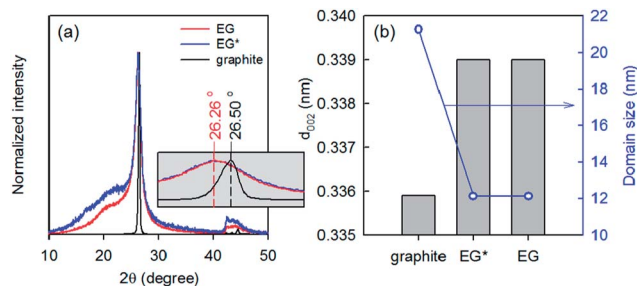


Fig. 2 Crystallographic characterization. (a) X-ray diffraction patterns. The intensities were normalized by that of the (002) peak of the corresponding material. (b) Comparison of  $d$ -spacing values and domain sizes. The values were calculated from the  $2\theta$  location and full width at half maximum of the (002) peak by using Bragg's law and Scherrer equation, respectively.

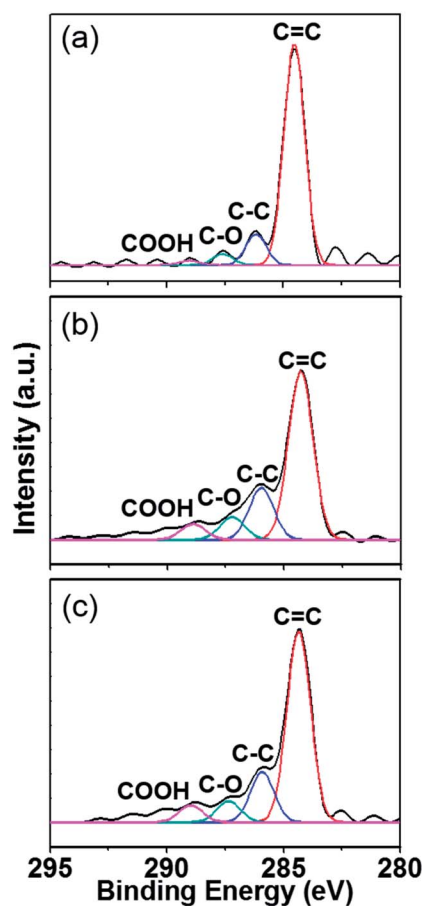


Fig. 3 C1s photoemission spectra of graphite (a), EG\* (b) and EG (c).

irregularly.<sup>5</sup> The representative  $d$ -spacing estimated at the (002) peak by the Bragg equation was changed from 0.3359 nm for the bare graphite to 0.3395 nm for EG\*. The  $d$ -spacing distribution is responsible for the broadness of the (002) peak of EG\* and the shoulder in its left between  $20^\circ$  and  $25^\circ$ . The domain size of the crystallites was accordingly reduced to half. After the subsequent thermal reduction, the  $2\theta$  location and broadness of the (002) peak and its left shoulder were not significantly changed.

Only the crystallographic difference between EG\* and EG was the relative portion of the shoulder to the (002) peak: the portion of larger  $d$ -spacing was discouraged by the thermal treatment at  $150^\circ\text{C}$  as graphitization proceeded.

Development of functional groups during the mild oxidation was clearly observed in C1s photoemission spectra (Fig. 3a and b and Table 1). A portion of double bonds between carbons in the  $\text{sp}^2$  hybrid configuration of graphite is oxidized into oxygen-containing functional groups (indicated by the increases of C–O and COOH), leaving single bonds between carbons indicating the  $\text{sp}^3$  configuration (indicated by the decrease in C=C and the increase in C–C). Formation of the functional groups is thought to be the main driving force to expand the distance between graphitic layers in graphite.<sup>5,15,16</sup> The chemical exfoliation of graphite into graphene oxide, achieved by severe oxidation, is the extreme case in which a large number of functional groups tethered to graphitic layers exhibits repulsive forces between the layers. In our mild oxidation, however, the layered structure of bare graphite was maintained macroscopically only with inter-layer distance changing. After the subsequent thermal reduction (Fig. 3b and c and Table 1), the C=C bonds between carbons indicating the  $\text{sp}^2$  hybrid configuration were partially recovered while C–C bonds as well as other functional groups were slightly decreased. Elemental analysis based on a combustion method supported the reduction of functional groups during the thermal reduction: O/C molar ratio = 0.094 (EG\*) versus 0.065 (EG).

Raman spectroscopy was used to investigate the structural transformation in terms of the degree of graphitization (Fig. 4). An additional D band (disorder band) appeared in EG\* and EG while only a sharp peak of the G band (graphite band) was observed in the bare graphite. The mild oxidation caused disorder by forming defects from the breakage of  $\text{sp}^2$  configuration and formation of functional groups as detected in the XPS study. Also, the G band was broadened and blue-shifted to higher wavenumber in EG\* (Fig. 4) as the amorphization by oxidation proceeds. The broadening of the G band results from vibrational states dispersed by bond-bending disorder or softening of non-six-fold rings.<sup>17</sup> There are several suggested explanations for the blue shift. When defects are developed in graphite, a new band called D' appears at  $\sim 1620\text{ cm}^{-1}$  and merged with the existing G band.<sup>18</sup> Also, the G band is blue-shifted from  $1581\text{ cm}^{-1}$  to  $1585\text{ cm}^{-1}$  when the attractive forces between graphitic layers are weakened.<sup>19</sup> After the subsequent thermal reduction, the intensity of the G band of EG increased

Table 1 Compositions of chemical bonds relevant to carbon estimated from C1s photoemission spectra in Fig. 3

		C=C	C–C	C–O	COOH
Graphite	Position (eV)	284.5	268.1	287.6	289.0
	Area (%)	82.7	11.6	4.1	1.6
EG*	Position (eV)	284.3	286.0	287.2	288.9
	Area (%)	65.2	20.4	8.6	5.8
EG	Position (eV)	284.4	286.0	287.4	288.9
	Area (%)	68.5	18.0	7.5	6.0

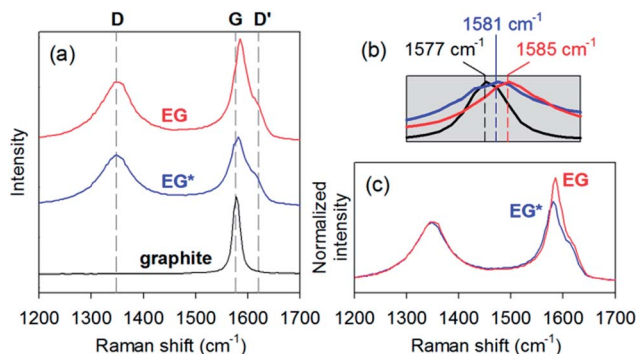


Fig. 4 Characterization of graphitization by Raman spectra. (a) Raw data. Three different bands (G, D and D') were indicated by dashed lines. (b) Comparison of Raman shifts at peaks of the G band. The same colours of the corresponding samples were used in (a). (c) Comparison between EG\* and EG by normalizing intensities by that of the D band.

compared with that of EG\* (Fig. 4c), implying that the degree of graphitization was partially redeemed.

Based on the *d*-spacing expansion by the mild oxidation and the redeemed graphitization by the subsequent thermal reduction, enhancement of lithium ion movement within interlayer channels is expected. To confirm and prove the improved kinetics, electrochemical performances were evaluated at different current rates (Fig. 5). During delithiation at 0.1 C, the expanded graphites (EG and EG\*) exhibited capacities at 290 and 183 mA h g<sup>-1</sup> respectively lower than that of graphite at 365 mA h g<sup>-1</sup> near the theoretical capacity of graphite. No significant decrease of capacity from the value at 0.1 C ( $Q_{0.1C}$ ) was observed until 10 C for all samples. The capacities of EG and EG\* were maintained close to their  $Q_{0.1C}$  (90% and 85% at 30 C) even after 30 C while that of bare graphite rapidly decreased to 68% of its  $Q_{0.1C}$  at 30 C. The gap of relative % capacities between the expanded and bare graphites was more intensified as the delithiation rates reached up to 50 C: 84% for EG and 77% for EG\* versus 18% for the bare graphite. Even in terms of the capacity

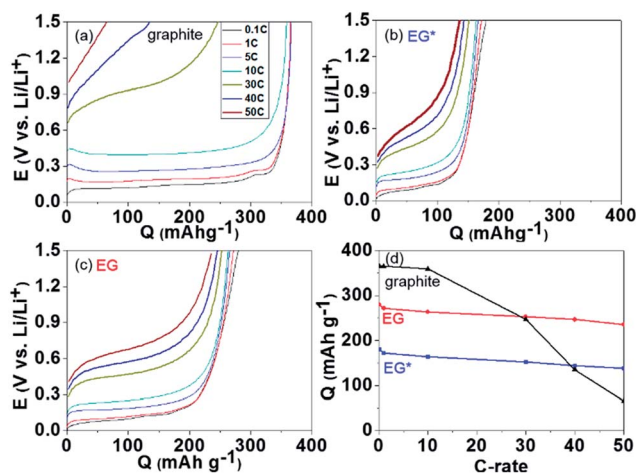


Fig. 5 Galvanostatic delithiation at different current rates. (a to c) Potential profiles of the bare graphite (a), EG\* (b) and EG (c). (d) C-rate dependency of capacities.

values in mA h g<sup>-1</sup>, EG\* and EG overcame their demerits of low initial capacities from 30 C and 40 C respectively.

The available capacity (assumed to be  $Q_{0.1C}$ ) of the expanded graphites inferior to that of the bare graphite can be explained by several reasons. Functional groups on the basal planes and more dominantly at the edges of graphitic layers trap lithium ions, resulting in larger irreversible capacities.<sup>20</sup> Also, more amount of solid-electrolyte interface (SEI) films are formed due to the electrochemical activity of surface defects of graphitic sheets and the larger surface area of expanded structures, leading to irreversible lithium ion storage.<sup>21</sup> The integrated area of EG in its differential capacity curve, which is proportional to the amount of SEI layer formation, was estimated to be ten times larger than that of bare graphite (Fig. S1†). The sp<sup>3</sup> carbon configuration is considered as another possible reason. The bare graphite is composed of sp<sup>2</sup> carbons which fully contribute to the capacity. However, both EG\* and EG contain not only sp<sup>2</sup> carbons but also sp<sup>3</sup> carbons that may not generate the LiC<sub>6</sub> complex during lithiation.

From the kinetic viewpoint, however, it is clear that lithium ion movement in the expanded graphites was faster than that in the bare graphite. Four reasons can be provided. Both EG\* and EG have wider channels through which lithium ions travel, which is indicated by the *d*-spacing increase after the mild oxidation. Smaller domain size of graphitized crystallites is also a helpful factor by shortening the ionic diffusion length. Thinner SEI layers of EG\* and EG than that of bare graphite facilitate lithium ion transport. The thickness of the SEI layer was characterized by depth profiles of X-ray photoelectron spectroscopy (XPS) and time-of-flight secondary ion mass spectrometry (TOF-SIMS). A dramatic increase of the atomic concentration of carbon is detected at the interface between the SEI layer and graphite. The intensity of the carbon-related XPS peak of EG\* and EG gradually increased after 10 min sputtering. In contrast, no significant change in the peak was observed with bare graphite even after 30 min sputtering. It implies that the SEI layer of bare graphite is much thicker than EG\* and EG. The depth profile of TOF-SIMS more clearly supports development of the thinner SEI layer of EG\* and EG (Fig. S3†). The concentration of carbon was saturated after 300 s in bare graphite while saturated earlier in EG\* and EG. It should be noted that the larger amount of the SEI layer of the expanded graphites is not contradictory to the thinner SEI layer development on the same materials because EG\* and EG provide higher surface areas exposed to the electrolyte than bare graphite. The fourth reason is based on the polarized-charge dispersion model suggested by Wang *et al.*<sup>22</sup> By our mild oxidation, the C–C bonds (therefore, C–H bonds) and other functional groups containing C–OH and COOH were developed. The hydrogen-containing bonds in functional groups are polarized through the electrostatic interactions or hydrogen bonding between the hydrogen atoms belonging to graphites and highly electronegative oxygen atoms of carbonate solvent molecules in the electrolyte. Consequently, partially induced negativity of carbons in graphite reduces the energy barrier of lithium ion intercalation.

Fig. 6a shows potential profiles of EG\* and EG at the first and the second cycle. At the first cycle, the expanded graphites

showed profiles similar to hydrogen-containing carbon materials.<sup>23</sup> The plateau around 0.8 V during lithiation is related to the SEI layer formation due to decomposition of EC in the electrolyte.<sup>24</sup> Once the SEI layer was formed at the first lithiation process, the plateau at 0.8 V was not observed during the second lithiation. Below 0.8 V, lithium ions are stored on or in graphites based on two different mechanisms. First, lithium ions are stored in the surface defects of EG\* and EG. A portion of lithium ions are consumed at this process, resulting in irreversibility.<sup>10,21</sup> Second, lithium ions are inserted or intercalated between graphitic layers. After the first lithiation, the reversibility of lithiation/delithiation was guaranteed with EG\* and EG (Fig. 6b). The capacity of both EG\* and EG was maintained up to higher than 95% of the capacity at the first cycle even after 100 cycles.

Lithiation of the bare graphite proceeds stage by stage (Fig. 6c).<sup>23</sup> Lithium ions are inserted into the empty inter-spacing layers where the energy barriers of intercalation are minimized. If all inter-spacing layers were identically defined, lithium ions would be intercalated in a way that minimizes the interaction between Li<sup>+</sup>-filled layers. Therefore, Li<sup>+</sup>-filled layers are periodically generated. Subsequently, lithium ions seek the layers for intercalation far away from the layers at which lithium ions are already filled. The periodicities of the filled layer determine the stages: *e.g.* stage 4 means lithium ions were intercalated every four layers (numbers in blue in Fig. 6c). Each stage transition is identified by its own electrochemical potential that is distinguished from the other stage transition (blue vertical lines). The stage behavior of the bare graphite was clearly observed in the differential capacity (dQ/dV) curve (Fig. 6c).

However, lithiation/delithiation behavior of EG was deviated from the well-defined staging behavior. The plateau potentials

were not clearly defined so that the peaks responsible for the stage transitions in the dQ/dV curve were broadened. The peak broadness originates from the *d*-spacing distribution as well as the irregular structure of EG compared with the bare graphite. Also, the potentials at which stages are changed were shifted to the negative direction of potential. During lithiation, lithium species move sluggishly inside EG due to slow electron supply caused by its lower electric conductivity even if the wider *d*-spacing of EG facilitates the insertion of lithium ions through the entrance of graphites. Lithium ions are stuck nearby the edge region, resulting in an intercalation potential shift to the negative direction (more overpotential). During delithiation, in contrast, lithium ions can be deintercalated in an easier way through the wider *d*-spacing gate, opening the pathway for their slow followers. Therefore, the deintercalation potential of EG is still more negative (less overpotential) compared with that of bare graphite. Fig. 6d strongly supports the asymmetric overpotential of EG between lithiation and delithiation by comparing differential capacity curves between two different C-rates. At a higher C-rate (0.5 C) with respect to a lower C-rate (0.1 C), a larger overpotential (more than 100 mV) indicated by the negative shift of the first lithiation potential was observed during lithiation while only a small overpotential (~10 mV) was investigated during delithiation. The C-rate dependency of the lithiation processes also confirmed the asymmetric behavior of overpotential of EG (Fig. S4†). The serious decrease of lithiation capacity is contrasted with a relatively insignificant change in delithiation capacity (Fig. 5d).

Electrochemical impedance spectra (EIS) were measured *in situ* every 10 min during delithiation at 0.1 C (Fig. 7). The size of semicircles of both EG and bare graphite gradually decreased as delithiation progressed. The depressed semicircles in the Nyquist plot result from overlapping of charge transfer processes at the two different interfaces in electrolyte|SEI layer|graphite systems. At the initial period of delithiation (SOC = 100%), EG fully utilized its kinetic advantage caused by wider channels. Smaller resistance (size of the semicircle) was involved with EG at the first time (as soon as delithiation began) when compared with that of the bare graphite. As delithiation proceeds, the effects of larger *d*-spacing of the expanded graphites on kinetics decrease. From 95% of state of charge (SOC), the sizes of semicircles were reversed between EG and

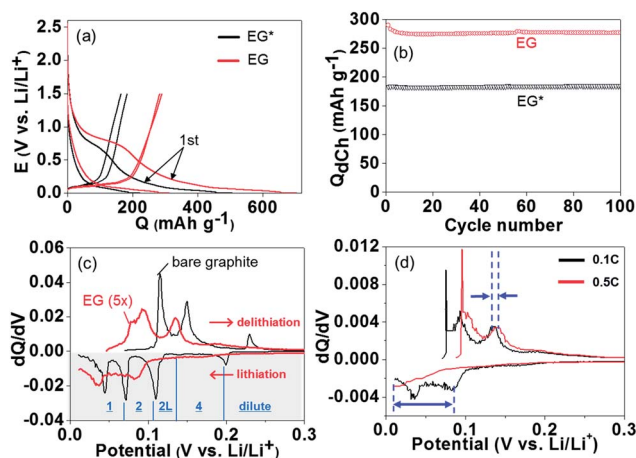


Fig. 6 (a) Potential profiles of EG\* and EG at the first and second cycles during lithiation at 0.1 C and delithiation at 0.1 C. (b) Capacity retention of EG\* and EG along cycles consisting of lithiation at 0.1 C followed by delithiation at 0.1 C. (c) Differential capacity curves of the bare graphite and EG at the second cycle. The red arrows indicate the potential scan directions. Stages were indicated in blue. (d) Differential capacity curves of EG at 0.1 C and 0.5 C. The gaps between blue dotted lines mean the overpotential.

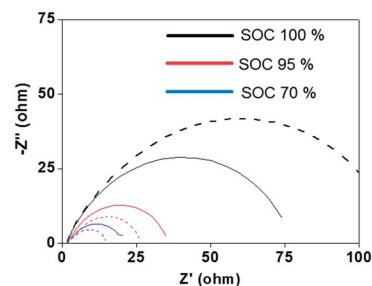


Fig. 7 Electrochemical impedance spectra of the bare graphite (dotted lines) and EG (solid lines) measured *in situ* during galvanostatic delithiation at 0.1 C.

the bare graphite. That is to say, the bare graphite became kinetically superior to EG after the critical state of charge (SOC) at the latter part of delithiation. The discussion also explains why the expanded graphites (EG\* or EG) are superior to the bare graphite especially at very high rates such as 50 C. It should be noted that the resistances estimated from the diameter of semicircles are the function of C-rates when impedance spectra are measured *in situ* during galvanostatic delithiation or lithiation (our preliminary experiments). The effective resistances estimated from the diameter of semicircles are expected to be smaller with EG than bare graphite in the SOC range of full delithiation at 30 C to 50 C even if it is difficult to measure them due to instrumentation limits (impedance spectra cannot be measured *in situ* within the time period (72 s) of full delithiation at 50 C). At the high rates, only the SOC range favorable to EG could be utilized without using the latter part of delithiation in which EG is inferior to the bare graphite.

## Conclusions

In this work, the effects of *d*-spacing and functional groups on electrochemical performances of graphite were investigated. The *d*-spacing between graphitic layers was controlled by oxidizing graphite in a mild degree at which the  $\pi$ - $\pi$  stacking was maintained without exfoliation. In the subsequent thermal reduction, the degree of graphitization was partially redeemed. Simultaneously, oxygen-containing functional groups were generated at edges or planes of graphite in the first oxidation step and then removed by the second reduction step. The expanded graphites (EG\* and EG) were lithiated/delithiated *via* intercalation/de-intercalation basically like graphite, which is distinguished from the adsorption mechanism shown in graphite oxide or graphene oxide. They exhibited enhanced capacities especially at fast rates over 30 C when compared with the original graphite. The larger *d*-spacing facilitated lithium ion movement between graphitic layers. Also, functional groups at the edges of graphite induced polarization of charge, decreasing activation energy required to extract lithium ions from graphite. We believe that modification of graphite opens a new possibility of old-fashioned but still dominantly used graphite anodes especially at high-rate applications. Even in the cases of silicon-graphite composites for higher capacities, high current cannot be extracted from silicon as a high-energy component. Only the modified graphites such as EG\* and EG shown in this work would cover the high-rate performances.

## Acknowledgements

This work was supported by MOTIE (Green: 10042948 (KEIT)), MSIP (Mid: 2013R1A2A2A04015706 (NRF), CRC: 2013K000210), MOE (BK21Plus: 10Z20130011057) and Korea Institute of Energy Research (no. GP2012-0024-03), Korea.

## Notes and references

- 1 A. Manthiram, in *Lithium Batteries: Science and Technology*, ed. G.-A. Nazri and G. Pistoia, Springer, New York, 2009, p. 35.
- 2 T. H. Kim, J. S. Park, S. K. Chang, S. Choi, J. H. Ryu and H. K. Song, *Adv. Energy Mater.*, 2012, **2**, 860.
- 3 N. Ding, J. Xu, Y. Yao, G. Wegner, X. Fang, C. Chen and I. Lieberwirth, *Solid State Ionics*, 2009, **180**, 222.
- 4 R. Ruffo, S. S. Hong, C. K. Chan, R. A. Huggins and Y. Cui, *J. Phys. Chem. C*, 2009, **113**, 11390.
- 5 J.-S. Park, M.-H. Lee, I.-Y. Jeon, H.-S. Park, J.-B. Baek and H.-K. Song, *ACS Nano*, 2012, **6**, 10770.
- 6 R. Tossici, M. Berrettoni, M. Rosolen and R. Marassi, *J. Electrochem. Soc.*, 1997, **144**, 186.
- 7 Y. Ein-Eli and V. R. Koch, *J. Electrochem. Soc.*, 1997, **144**, 2968.
- 8 C. Menachem, Y. Wang, J. Flowers, E. Peled and S. G. Greenbaum, *J. Power Sources*, 1998, **76**, 180.
- 9 E. Yoo, J. Kim, E. Hosono, H.-s. Zhou, T. Kudo and I. Honma, *Nano Lett.*, 2008, **8**, 2277.
- 10 H. F. Xiang, Z. D. Li, K. Xie, J. Z. Jiang, J. J. Chen, P. C. Lian, J. S. Wu, Y. Yu and H. H. Wang, *RSC Adv.*, 2012, **2**, 6792.
- 11 A. Mukhopadhyay, F. Guo, A. Tokranov, X. Xiao, R. H. Hurt and B. W. Sheldon, *Adv. Funct. Mater.*, 2013, **23**, 2397.
- 12 S. You, B. Sundqvist and A. V. Talyzin, *ACS Nano*, 2013, **7**, 1395.
- 13 S. Stankovich, D. A. Dikin, R. D. Piner, K. A. Kohlhaas, A. Kleinhammes, Y. Jia, Y. Wu, S. T. Nguyen and R. S. Ruoff, *Carbon*, 2007, **45**, 1558.
- 14 K. Jo, T. Lee, H. J. Choi, J. H. Park, D. J. Lee, D. W. Lee and B.-S. Kim, *Langmuir*, 2011, **27**, 2014.
- 15 M. J. McAllister, J.-L. Li, D. H. Adamson, H. C. Schniepp, A. A. Abdala, J. Liu, M. Herrera-Alonso, D. L. Milius, R. Car and R. K. Prud'homme, *Chem. Mater.*, 2007, **19**, 4396.
- 16 Y.-R. Shin, S.-M. Jung, I.-Y. Jeon and J.-B. Baek, *Carbon*, 2012, **50**, 1465.
- 17 A. C. Ferrari and J. Robertson, *Phys. Rev. B: Condens. Matter Mater. Phys.*, 2000, **61**, 14095.
- 18 K. N. Kudin, B. Ozbas, H. C. Schniepp, R. K. Prud'homme, I. A. Aksay and R. Car, *Nano Lett.*, 2008, **8**, 36.
- 19 D. Graf, F. Molitor, K. Ensslin, C. Stampfer, A. Jungen, C. Hierold and L. Wirtz, *Nano Lett.*, 2007, **7**, 238.
- 20 G.-A. Nazri and B. Yebka, in *Materials for Lithium-Ion Batteries*, ed. C. Julien and Z. Stoyanov, Kluwer Academic Publishers, The Netherlands, 2000, p. 162.
- 21 D. Y. Pan, S. Wang, B. Zhao, M. H. Wu, H. J. Zhang, Y. Wang and Z. Jiao, *Chem. Mater.*, 2009, **21**, 3136.
- 22 S. Wang, Y. Zhang, L. Yang and Q. Liu, *Solid State Ionics*, 1996, **86**, 919.
- 23 M. Winter, J. O. Besenhard, M. E. Spahr and P. Novak, *Adv. Mater.*, 1998, **10**, 725.
- 24 M. Nazri, B. Yebka and G.-A. Nazri, in *Lithium Batteries: Science and Technology*, ed. G.-A. Nazri and G. Pistoia, Springer, New York, 2009, p. 203.